

# Massive Right-handed Neutrinos in B Decays

Hongkai Liu

Department of Physics, Technion – Israel Institute of Technology, Haifa 3200003, Israel

In this paper, we present the differential decay distributions for  $\bar{B} \rightarrow D^{(*)} \ell \bar{X}$  decays with a massive right-handed neutrino in the low-energy effective field theory framework and show how the massive effects of the RH neutrinos can explain the positive value of the difference in forward-backward asymmetries,  $\Delta A_{FB} \equiv A_{FB}^\mu - A_{FB}^e$ , tentatively inferred from Belle data. We also make predictions for  $q^2$  dependent angular observables to motivate future measurements.

## I. INTRODUCTION

The recently noticed  $4\sigma$  deviation from the standard model (SM) predictions in the difference of the forward-backward asymmetry between the muon and electron channel ( $\Delta A_{FB} \equiv A_{FB}^\mu - A_{FB}^e$ ) measured from Belle data in Ref. [1] motivates the new physics (NP) in the electron and muon sector. The anomalies in the  $\Delta$  observables are quite interesting, as they have very little form factor uncertainties and hence any measured deviations from the SM predictions for these observables would be clear signs of NP.

Massive right-handed (RH) or sterile neutrinos are well-motivated hypothetical particles to explain many phenomena beyond the standard model (BMS), such as neutrino oscillations and dark matter. RH neutrinos are sterile under the SM gauge interactions and can be incorporated into the standard model effective field theory (SMEFT). The resulting EFT [2–6], called SMNEFT, includes additional interactions of the RH neutrinos with SM fields. The mass scale of the RH neutrino can vary over a large range. We consider the case of a light RH neutrino so that it appears as an explicit degree of freedom in the EFT framework. The differential decay distribution for  $\bar{B} \rightarrow D \ell \bar{\nu}$  with a massless RH neutrino is given in Ref. [7]. We generalize the result for a nonzero RH neutrino mass  $m_N$ . A finite  $m_N$  affects both the phase space and the leptonic helicity amplitudes. Given the anomalies in the measured value of  $(g-2)_\mu$  [8] and neutral-current  $b \rightarrow s \mu^+ \mu^-$  decays [9], we assume the massive RH neutrinos can be produced from B meson decays and couple to the muon sector to explain the anomaly in  $\Delta A_{FB}$ .

## II. FRAMEWORK

The  $B$  charged-current decay  $b \rightarrow c \ell \bar{X}$  can be described by the operators in the low-energy effective field theory (LEFT)

$$-\mathcal{L}_{\text{eff}} = \frac{4G_F V_{cb}}{\sqrt{2}} (\mathcal{O}_{LL}^V + \sum_{\substack{X=S,V,T \\ \alpha,\beta=L,R}} C_{\alpha\beta}^X \mathcal{O}_{\alpha\beta}^X), \quad (1)$$

TABLE I: The origin of low-energy effective operators from SMNEFT.

$\mathcal{O}_{\ell q}^{(3)}$	$\mathcal{O}_{\ell equ}^{(1)}$	$\mathcal{O}_{\ell edq}$	$\mathcal{O}_{\ell eqd}^{(3)}$	$\mathcal{O}_{nedu}$	$\mathcal{O}_{\ell nuq}$	$\mathcal{O}_{\ell nqd}^{(1)}$	$\mathcal{O}_{\ell nqd}^{(3)}$
$\mathcal{O}_{LL}^V$	$\mathcal{O}_{LL}^S$	$\mathcal{O}_{RL}^S$	$\mathcal{O}_{LL}^T$	$\mathcal{O}_{RR}^V$	$\mathcal{O}_{LR}^S$	$\mathcal{O}_{RR}^S$	$\mathcal{O}_{RR}^T$

where

$$\mathcal{O}_{\alpha\beta}^V \equiv (\bar{c} \gamma^\mu P_\alpha b) (\bar{\ell} \gamma^\mu P_\beta X), \quad (2)$$

$$\mathcal{O}_{\alpha\beta}^S \equiv (\bar{c} P_\alpha b) (\bar{\ell} P_\beta X), \quad (3)$$

$$\mathcal{O}_{\alpha\beta}^T \equiv \delta_{\alpha\beta} (\bar{c} \sigma^{\mu\nu} P_\alpha b) (\bar{\ell} \sigma_{\mu\nu} P_\beta X), \quad (4)$$

with  $X$  the left-handed (LH) SM neutrinos or RH neutrinos. The SM and NP contributions are in the first and second terms in Eq. (1), respectively. After matching at the electroweak scale, only the operators  $\mathcal{O}_{LL}^V$ ,  $\mathcal{O}_{LL}^S$ ,  $\mathcal{O}_{RL}^S$ , and  $\mathcal{O}_{LL}^T$  can arise from the four-fermion operators in SMEFT, while SMNEFT yields four more operators:  $\mathcal{O}_{RR}^V$ ,  $\mathcal{O}_{LR}^S$ ,  $\mathcal{O}_{RR}^S$ , and  $\mathcal{O}_{RR}^T$ ; see Table I. Note that  $\mathcal{O}_{LR}^V$  and  $\mathcal{O}_{RL}^V$  cannot be produced from the four-fermion operators in SMNEFT. The renormalization group running of the operators from  $\Lambda$  to  $m_Z$  and then down to the  $m_b$  scale has been discussed in Refs. [10, 11]. In what follows, we work in the LEFT framework keeping in mind that the corresponding SMNEFT WCs can be obtained by carrying out the running and matching.

## III. PHENOMENOLOGY

The differential decay distribution for  $\bar{B} \rightarrow D \ell \bar{X}$  can be expressed in terms of the three  $\mathcal{J}$  functions as

$$\frac{d^2 \Gamma_D}{dq^2 d \cos \theta_\ell} = \mathcal{J}_0(q^2) + \mathcal{J}_1(q^2) \cos \theta_\ell + \mathcal{J}_2(q^2) \cos^2 \theta_\ell, \quad (5)$$

with  $q^2 \equiv (p_\ell + p_{\bar{X}})^2$  and  $\theta_\ell$  the angle between the charged lepton momentum in the  $\ell \bar{X}$  rest frame and the direction of the  $D$  momentum in the  $\bar{B}$  rest frame. The differential decay width and angular observable

$A_{FB}$  can be written in terms of  $\mathcal{J}$  functions

$$\Gamma_f^D(q^2) \equiv \frac{d\Gamma_D}{dq^2} = 2\mathcal{J}_0(q^2) + \frac{2}{3}\mathcal{J}_2(q^2), \quad (6)$$

$$A_{FB}^D(q^2) \equiv -\frac{\mathcal{J}_1(q^2)}{d\Gamma_D/dq^2}. \quad (7)$$

Similarly, the differential decay distribution for  $\bar{B} \rightarrow D^*(\rightarrow D\pi)\ell\bar{X}$  with nonzero  $m_N$ , can be written in terms of the 12 different angular structures that appear in the massless RH neutrino case:

$$\begin{aligned} \frac{8\pi}{3} \frac{d^4\Gamma_{D^*}}{dq^2 d\cos\theta_\ell d\cos\theta_D d\phi} = & (\mathcal{I}_{1s} + \mathcal{I}_{2s} \cos 2\theta_\ell + \mathcal{I}_{6s} \cos \theta_\ell) \sin^2 \theta_D \\ & + (\mathcal{I}_{1c} + \mathcal{I}_{2c} \cos 2\theta_\ell + \mathcal{I}_{6c} \cos \theta_\ell) \cos^2 \theta_D \\ & + (\mathcal{I}_3 \cos 2\phi + \mathcal{I}_9 \sin 2\phi) \sin^2 \theta_D \sin^2 \theta_\ell \\ & + (\mathcal{I}_4 \cos \phi + \mathcal{I}_8 \sin \phi) \sin 2\theta_D \sin 2\theta_\ell \\ & + (\mathcal{I}_5 \cos \phi + \mathcal{I}_7 \sin \phi) \sin 2\theta_D \sin \theta_\ell, \end{aligned} \quad (8)$$

where the three angles are defined in Fig. 1. The expression of  $\mathcal{J}$  and  $\mathcal{I}$  functions are quite lengthy as they depend on the WCs, mass of RH neutrinos,  $q^2$ , and hadronic form factors. We do not present the details of those angular functions in this paper for brevity. For the complete expression see *Supplemental Material* in Ref. [12]. We adopt the hadronic form factors of Ref. [13] including the corrections up to  $1/m_c^2$  in the heavy-quark limit. The  $q^2$  distributions of differential decay width and angular observables are related to the angular functions as follow

$$\begin{aligned} \Gamma_f^{D^*}(q^2) \equiv \frac{d\Gamma_{D^*}}{dq^2} = & 2\mathcal{I}_{1s}(q^2) + \mathcal{I}_{1c}(q^2) \\ & - \frac{1}{3}(2\mathcal{I}_{2s}(q^2) + \mathcal{I}_{2c}(q^2)). \end{aligned}$$

$$A_{FB}^{D^*}(q^2) = -\frac{\mathcal{I}_{6s}(q^2) + \frac{1}{2}\mathcal{I}_{6c}(q^2)}{\Gamma_f^{D^*}(q^2)}, \quad (9)$$

$$F_L(q^2) = \frac{\mathcal{I}_{1c}(q^2) - \frac{1}{3}\mathcal{I}_{2c}(q^2)}{\Gamma_f^{D^*}(q^2)}, \quad (10)$$

$$\tilde{F}_L(q^2) = \frac{1}{3} - \frac{8}{9} \frac{2\mathcal{I}_{2s}(q^2) + \mathcal{I}_{2c}(q^2)}{\Gamma_f^{D^*}(q^2)} \quad (11)$$

$$S_i(q^2) = \frac{\mathcal{I}_i(q^2)}{\Gamma_f^{D^*}(q^2)}. \quad (12)$$

To compare with experimental measurements, we define 9 bins of the normalized  $q^2$ -distributions [14],

$$\Delta x_i^{D^{(*)}} \equiv \frac{1}{\Gamma_{\text{tot}}^{D^{(*)}}} \int_{q_{i-1}^2}^{q_i^2} dq^2 \Gamma_f^{D^{(*)}}(q^2), \quad i = 2 \text{ to } 10 \quad (13)$$

where  $\Gamma_{\text{tot}}^{D^{(*)}}$  is the total decay width after integrating  $\Gamma_f^{D^{(*)}}(q^2)$  over the entire range of  $q^2$ . The  $q^2$  bins are defined by

$$q_i^2 \equiv m_B^2 + m_{D^{(*)}}^2 - 2m_B m_{D^{(*)}} \omega_i, \quad i = 1 \text{ to } 10, \quad (14)$$

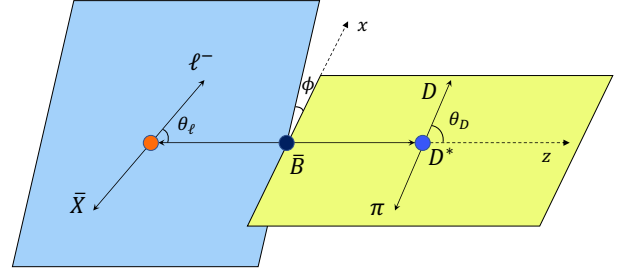


FIG. 1: Kinematic variables for  $\bar{B} \rightarrow \ell^- \bar{X} D^*(\rightarrow D\pi)$ .

with  $\omega_i = 1 + i/20$ . The  $q^2$ -binned and -averaged observables are defined by

$$O_i \equiv \frac{1}{\Gamma_{\text{tot}}^{D^{(*)}}} \int_{q_{i-1}^2}^{q_i^2} dq^2 O(q^2) \Gamma_f^{D^{(*)}}(q^2), \quad i = 2 \text{ to } 10, \quad (15)$$

$$\langle O \rangle \equiv \frac{1}{\Gamma_{\text{tot}}^{D^{(*)}}} \int_{q_{\text{min}}^2}^{q_{\text{max}}^2} dq^2 O(q^2) \Gamma_f^{D^{(*)}}(q^2). \quad (16)$$

The values of  $\langle A_{FB}^{D^*} \rangle$ ,  $\langle \tilde{F}_L \rangle$ ,  $\langle F_L \rangle$  and  $\langle S_3 \rangle$ , measured by the Belle experiment are listed in Table II. Measurements of the two ratios of branching fractions  $R_{D^{(*)}}^{\mu/e}$  are also listed in Table II.

We find that the nonzero RH neutrino mass produces significant effects in the angular observables which may explain the  $4\sigma$  tension in  $\Delta\langle A_{FB}^{D^*} \rangle$ . In Fig. 2, we show  $\Delta\langle A_{FB}^{D^*} \rangle$  as a function  $m_N$  for  $C_{RR}^S = C_{RR}^V = C_{RR}^T = 1$ . Clearly, a GeV RH neutrino with vector or tensor interactions can fit the  $\Delta\langle A_{FB}^{D^*} \rangle$  measurement within  $1\sigma$ . We observe that if the RH neutrino is massless,  $\Delta\langle A_{FB}^{D^*} \rangle$  is below the SM prediction. However, for  $m_N \simeq 1$  GeV, the  $\Delta\langle A_{FB}^{D^*} \rangle$  anomaly can be explained

TABLE II: Ten observables that are sensitive to NP in the  $\mu$  sector. The corresponding predictions for the three BPs of Table III are provided.

Observable	Measurement	BP1	BP2	BP3
$\Delta\langle A_{\text{FB}}^{D^*} \rangle$	$0.0349 \pm 0.0089$	0.0188	-0.0014	-0.0016
$\Delta\langle F_L \rangle$	$-0.0065 \pm 0.0059$	-0.0057	-0.0063	-0.0025
$\Delta\langle \tilde{F}_L \rangle$	$-0.0107 \pm 0.0142$	-0.0314	-0.0099	-0.0034
$\Delta\langle S_3 \rangle$	$-0.0127 \pm 0.0109$	0.0035	0.0049	0.0007
$R_D^{\mu/e}$	$0.995 \pm 0.022 \pm 0.039$	1.015	1.036	1.012
$R_{D^*}^{\mu/e}$	$0.99 \pm 0.01 \pm 0.03$	0.983	1.021	0.991
$\Delta x_2^{D^*}$	$-0.0040 \pm 0.0029$	-0.0153	-0.0022	-0.0002
$\Delta x_3^{D^*}$	$-0.0025 \pm 0.0033$	0.0	-0.0022	0.0001
$\Delta x_4^{D^*}$	$0.0024 \pm 0.0038$	0.0014	-0.0022	0.0002
$\Delta x_5^{D^*}$	$0.0043 \pm 0.0046$	0.0022	-0.0006	0.0002
$\Delta x_6^{D^*}$	$-0.0035 \pm 0.0052$	0.0027	0.0009	0.0003
$\Delta x_7^{D^*}$	$0.0066 \pm 0.0056$	0.0030	0.0018	0.0003
$\Delta x_8^{D^*}$	$-0.0103 \pm 0.0054$	0.0032	0.0021	0.0003
$\Delta x_9^{D^*}$	$0.0 \pm 0.0052$	0.0031	0.0020	0.0003
$\Delta x_{10}^{D^*}$	$0.0019 \pm 0.0044$	0.0028	0.0017	0.0003
$\Delta\langle A_{\text{FB}}^D \rangle$	-	0.0401	-0.0032	-0.0209
$\Delta\langle S_4 \rangle$	-	0.0121	0.0087	0.0021
$\Delta\langle S_5 \rangle$	-	-0.0128	-0.0051	0.0015

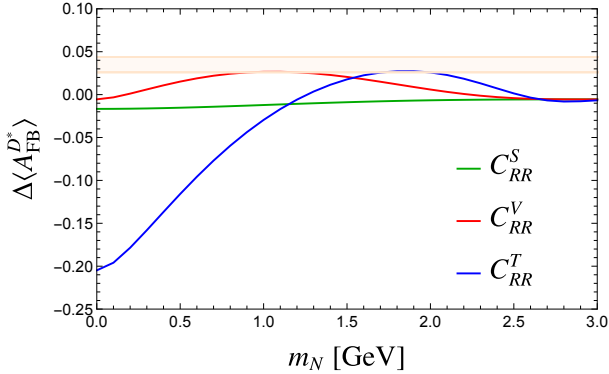


FIG. 2:  $\Delta\langle A_{\text{FB}}^{D^*} \rangle$  as a function of  $m_N$  for  $C_{RR}^S = C_{RR}^V = C_{RR}^T = 1$ . The light orange band shows the Belle measurement at  $1\sigma$ .

if  $C_{RR}^V = 1$  (red curve). For  $m_N \simeq 2$  GeV, the anomaly can be explained by  $C_{RR}^T = 1$ . However, these illustrative scenarios are excluded by other measurements in Table II. So, to reproduce the  $\Delta\langle A_{\text{FB}}^{D^*} \rangle$  anomaly and the other measurements in Table II, we choose three benchmark points (BPs) of Table III. BP1 has both LH and RH interactions, while BP2 and BP3 only have RH and LH interactions, respectively. The predictions for the three BPs for the 15 measurements are provided

in Table II and Fig. 3. Since there is no interference between LH and RH contributions, scenarios with only RH interactions (like BP2) necessarily increase  $R_D^{\mu/e}$  and  $R_{D^*}^{\mu/e}$ , and it is not possible to sufficiently enhance

	$m_N$ (GeV)	$C_{RR}^V$	$C_{RR}^S$	$C_{RR}^T$	$C_{LL}^V$	$C_{LL}^S$	$C_{LL}^T$
BP1	0.4	0.82	0.1	0.02	-0.4	0	0
BP2	1.6	0.15	-0.3	0.06	0	0	0
BP3	0	0	0	0	0	0.06	0.02

TABLE III: The parameters for three benchmark points. The WCs not listed are zero.

$\Delta\langle A_{\text{FB}}^{D^*} \rangle$ . Only LH interactions (BP3) are unable to adequately reproduce all the measurements.

We now calculate  $A_{\text{FB}}^{D^*}(q^2)$ ,  $\tilde{F}_L(q^2)$ ,  $F_L(q^2)$  and  $S_3(q^2)$  for our BP scenarios. We present the four binned angular observables for the three BPs in Fig. 3. We also show the normalized  $q^2$  distribution for  $\bar{B} \rightarrow D\ell\bar{X}$ . Large deviations from the SM are evident in several  $q^2$  bins. The error bars in the middle and lower panels indicate the uncertainties due to the hadronic form factors. We estimate these as the range of predictions using our chosen form factors [13] and the form factors of Refs. [15, 16]. We see that  $\Delta S_3$  is quite sensitive to the form factor.

Other observables that have not yet been measured and can be significantly modified by NP include the forward-backward asymmetry in  $\bar{B} \rightarrow D\ell\bar{X}$ ,  $A_{\text{FB}}^D$ . In the SM, this is suppressed by  $m_\ell^2$ . The  $q^2$  averaged values of  $\Delta A_{\text{FB}}^D$ ,  $\Delta S_4$  and  $\Delta S_5$  for the BPs are displayed in Table II. In Fig. 4, we plot the corresponding  $q^2$  binned observables and find that large deviations from the SM are possible.

#### IV. SUMMARY

We find that a nonzero  $m_N$  is needed to obtain a positive value of  $\Delta\langle A_{\text{FB}}^{D^*} \rangle$ , as suggested by Belle data. We also made predictions for several angular observables that differ substantially from SM expectations.

#### Acknowledgments

I thank Alakabha Datta and Danny Marfatia for collaboration on Ref. [12]. This work is supported by ISF, BSF and Azrieli foundation.

[1] E. Waheed et al. (Belle), Phys. Rev. D **100**, 052007 (2019), [Erratum: Phys.Rev.D 103, 079901 (2021)],

1809.03290.

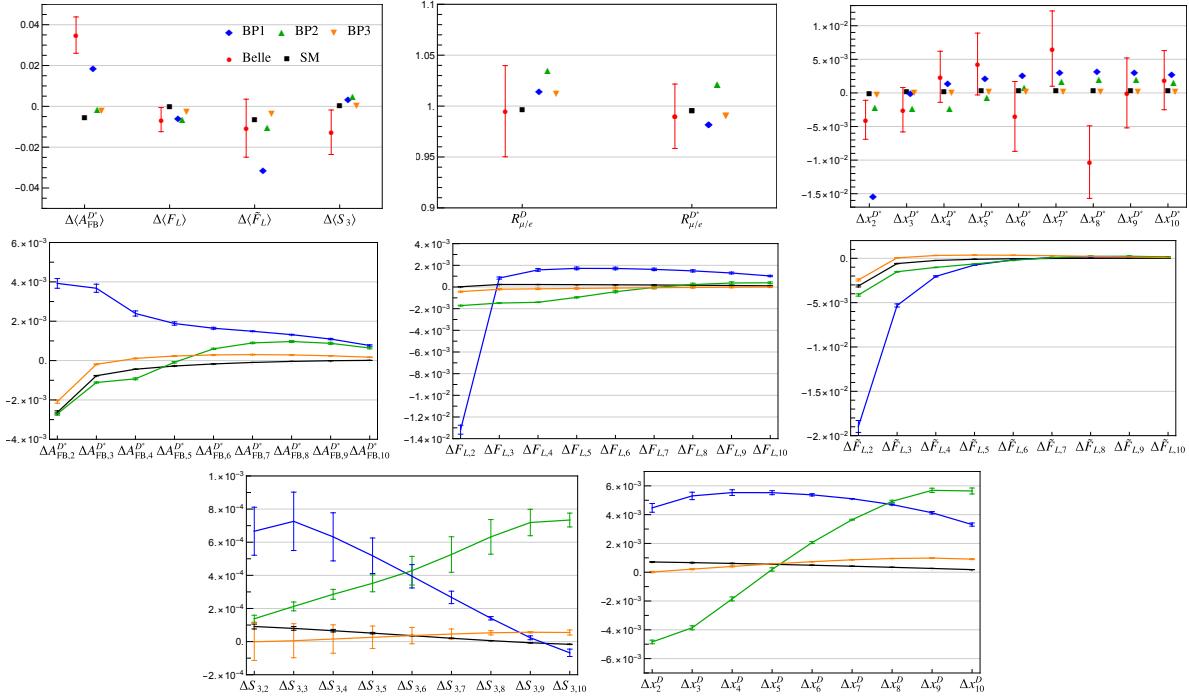


FIG. 3: The expectations for the SM and three BPs for the observables in the upper and middle panels of Table II. The Belle measurements are shown in the upper panels. The error bars in the middle and lower panels are hadronic form factor uncertainties.

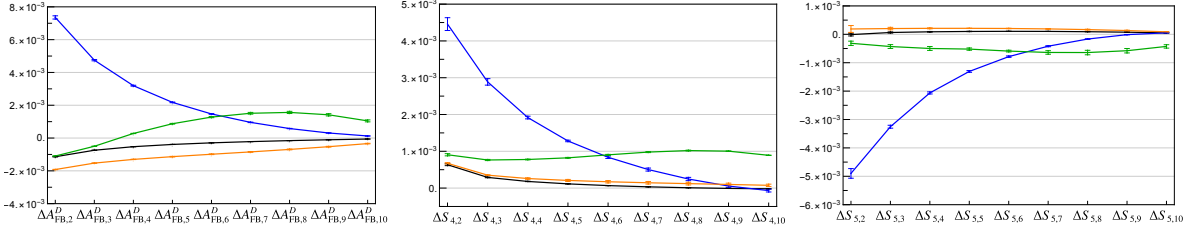


FIG. 4:  $q^2$  distributions of the three angular observables in the lower panel of Table II.

- [2] F. del Aguila, S. Bar-Shalom, A. Soni, and J. Wudka, Phys. Lett. B **670**, 399 (2009), 0806.0876.
- [3] A. Aparici, K. Kim, A. Santamaria, and J. Wudka, Phys. Rev. D **80**, 013010 (2009), 0904.3244.
- [4] S. Bhattacharya and J. Wudka, Phys. Rev. D **94**, 055022 (2016), [Erratum: Phys.Rev.D 95, 039904 (2017)], 1505.05264.
- [5] Y. Liao and X.-D. Ma, Phys. Rev. D **96**, 015012 (2017), 1612.04527.
- [6] I. Bischer and W. Rodejohann, Nucl. Phys. B **947**, 114746 (2019), 1905.08699.
- [7] R. Mandal, C. Murgui, A. Peñuelas, and A. Pich, JHEP **08**, 022 (2020), 2004.06726.
- [8] B. Abi et al. (Muon g-2), Phys. Rev. Lett. **126**, 141801 (2021), 2104.03281.
- [9] R. Aaij et al. (LHCb) (2021), 2103.11769.
- [10] A. Datta, J. Kumar, H. Liu, and D. Marfatia, JHEP **02**, 015 (2021), 2010.12109.
- [11] A. Datta, J. Kumar, H. Liu, and D. Marfatia, JHEP **05**, 037 (2021), 2103.04441.
- [12] A. Datta, H. Liu, and D. Marfatia (2022), 2204.01818.
- [13] M. Bordone, N. Gubernari, D. van Dyk, and M. Jung, Eur. Phys. J. C **80**, 347 (2020), 1912.09335.
- [14] C. Bobeth, D. van Dyk, M. Bordone, M. Jung, and N. Gubernari (2021), 2104.02094.
- [15] M. Tanaka and R. Watanabe, Phys. Rev. D **87**, 034028 (2013), 1212.1878.
- [16] S. Iguro and R. Watanabe, JHEP **08**, 006 (2020), 2004.10208.